Novel Isoniazid cocrystals with aromatic carboxylic acids: Crystal engineering, spectroscopy and thermochemical investigations

Article *in* Journal of Molecular Structure · September 2017

DOI: 10.1016/j.molstruc.2017.09.115

CITATION
1

READS
332

6 authors, including:

Luan F. Diniz

22 PUBLICATIONS **21** CITATIONS

SEE PROFILE

Matheus S. Souza

University of São Paulo

15 PUBLICATIONS **9** CITATIONS

SEE PROFILE

Paulo Carvalho Jr

National Nanotechnology Laboratory for Agribusiness

33 PUBLICATIONS **77** CITATIONS

SEE PROFILE

Cecilia Silva

University of São Paulo

28 PUBLICATIONS **151** CITATIONS

SEE PROFILE

Journal of Molecular Structure 1153 (2018) 58–68

Contents lists available at ScienceDirect

Journal of Molecular Structure

journal homepage: http://www.elsevier.com/locate/molstruc

Novel Isoniazid cocrystals with aromatic carboxylic acids: Crystal engineering, spectroscopy and thermochemical investigations

Luan F. Diniz [a], Matheus S. Souza [a], Paulo S. Carvalho Jr. [a], Cecilia C.P. da Silva [a], Richard F. D'Vries [a, b], Javier Ellena [a, *]

[a] Instituto de Física de São Carlos, Universidade de São Paulo, CP 369, 13560-970 São Carlos, SP, Brazil
[b] Universidad Santiago de Cali, Calle 5 # 62-00, Cali, Colombia

ARTICLE INFO

Article history:
Received 7 June 2017
Received in revised form
27 September 2017
Accepted 28 September 2017
Available online 30 September 2017

Keywords:
Tuberculosis
Isoniazid
Cocrystals
Crystal engineering
X-ray diffraction

ABSTRACT

Four novel cocrystals of the anti-tuberculosis drug Isoniazid (INH), including two polymorphs, with the aromatic carboxylic acids *p*-nitrobenzoic (PNBA), *p*-cyanobenzoic (PCNBA) and *p*-aminobenzoic (PABA) were rationally designed and synthesized by solvent evaporation. Aiming to explore the possible supramolecular synthons of this API, these cocrystals were fully characterized by X-ray diffraction (SCXRD, PXRD), spectroscopic (FT-IR) and thermal (TGA, DSC, HSM) techniques. The cocrystal formation was found to be mainly driven by the synthons formed by the pyridine and hydrazide moieties. In both INH–PABA polymorphs, the COOH acid groups are H-bonded to pyridine and hydrazide groups giving rise to the acid···pyridine and acid···hydrazide heterosynthons. In INH–PNBA and INH–PCNBA cocrystals these acid groups are only related to the pyridine moiety. In addition to the structural study, supramolecular and Hirshfeld surface analysis were also performed based on the structural data. The cocrystals were identified from the FT-IR spectra and their thermal behaviors were studied by a combination of DSC, TGA and HSM techniques.

1. Introduction

Multicomponent crystals, *e.g.* salts and cocrystals, are important technology topics in pharmaceutical science [1–3]. Cocrystals have been attracting scientific and pharmaceutical interest in the last decades due to their potential ability to modify important properties of active pharmaceutical ingredients (APIs) such as solubility, dissolution rate, bioavailability, hygroscopicity, and/or thermal stability. In addition, cocrystal formation does not lead to changes in the nature of the API, unlike the situation observed during salt formation, where the API must protonate or be protonated [3–7]. Since cocrystals are the result of a supramolecular synthesis and their physicochemical and pharmacokinetic properties are not predictable, they can be considered a novel and non-obvious invention. Consequently, cocrystals can be patented if they show some utility [4,8,9].

Isoniazid (INH, Scheme 1), pyridine-4-carbohydrazide, has been the subject of many scientific studies, not only due to its therapeutic properties, but also because of its ability to form a variety of solid forms [10–14]. This API is a bacteriostatic stable drug widely used in combination with Rifampicin (RMP), Pyrazinamide (PZA) and Ethambutol (ETB) as a fixed-dose combination (FDC) tablet in the first phase of tuberculosis (TB) treatment [15–17]. The use of four drugs in a single tablet aims to reduce the risk of drug-resistance and simplify the TB treatment [18]. Although INH is stable over long time periods at ambient temperature as well as in accelerated stability conditions (40 °C, 75% RH) [19,20], its main drawback is that, in the FDC tablet formulations, INH undergoes degradation due to drug-drug interactions [21,22]. The presence of other anti-TB drugs, such as PZA and ETB, were found to further accelerate the INH degradation [23]. Its limited stability in the FDC formulation has spurred the design of new solid forms, such as salts and cocrystals, in order to enhance it pharmaceutical behavior and solve its stability issue.

In the present study, pharmaceutical cocrystals of INH were synthesized by a crystal engineering approach with three aromatic carboxylic acids: *p*-nitrobenzoic acid (PNBA), *p*-cyanobenzoic acid (PCNBA), and *p*-aminobenzoic acid (PABA) (Scheme 1). In order to expand the range of new solid forms of INH available, an extensive amount of structures has been reported in the last few years

* Corresponding author.
E-mail address: javiere@ifsc.usp.br (J. Ellena).

https://doi.org/10.1016/j.molstruc.2017.09.115
0022-2860/

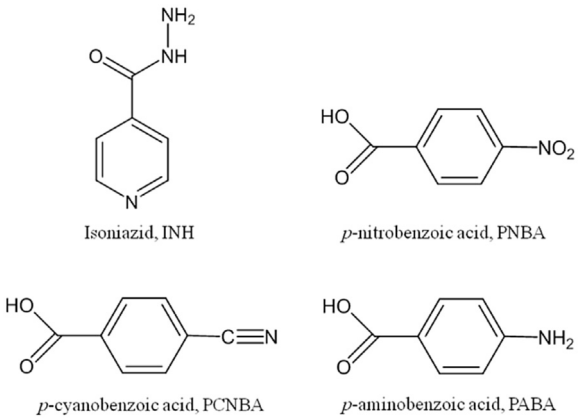

Scheme 1. Molecular structure of INH and coformers used in this study.

[24–29]. Recently, Trivedi et al. [30] reported a series of two salts and two cocrystals of INH with three coformers (2,5-dihydroxybenzoic, 3-aminobenzoic, and phthalic acids). Following this approach, in a previous, but recent study [31], our group synthetized and depicted four INH inorganic salts: a hydrobromide, a nitrate, an anhydrous sulfate, and an hemihydrate sulfate. Within this framework, the novel cocrystals described herein were planned with the aim of exploring the diversity of the supramolecular synthons of this API, and provide insights that might be useful for the future synthesis of INH crystalline structures with improved stability properties. The characterization of these cocrystals was carried out using Single-Crystal and Powder X-ray Diffraction (SCXRD, PXRD), Hirshfeld Surface (HS) Analysis, Thermogravimetric Analysis (TGA), Differential Scanning Calorimetry (DSC), Hot-Stage Microscopy (HSM) and Fourier Transform Infrared (FT-IR).

2. Experimental details

All reagents were purchased from Sigma-Aldrich and used without any further purification. Analytical grade solvents were used for the crystallization experiments. Cocrystals were crystallized via the technique of slow solvent evaporation.

2.1. Supramolecular synthesis of isoniazid cocrystals

a *INH–PNBA*. Isoniazid (*40 mg, 0.292 mmol*) and *p*-nitrobenzoic acid (48.6 mg, 0.291 mmol) were dissolved in 5 mL of ethanol and heated at 70 °C for 30 min. Colorless plates of the 1:1 INH–PNBA cocrystal were obtained at room temperature.

b *INH–PCNBA*. Isoniazid (*40 mg, 0.292 mmol*) and *p*-cyanobenzoic acid (42.8 mg, 0.291 mmol) were dissolved in a hot (70 °C) ethanol/acetonitrile (2:1 mixture) solution. Colorless plates of 1:1 INH–PCNBA cocrystal were obtained at room temperature.

c *INH–PABA*. Isoniazid (*40 mg, 0.292 mmol*) and *p*-aminobenzoic acid (80 mg, 0.584 mmol) were dissolved in a hot (70 °C) solution of ethanol/acetonitrile (2:1 mixture). Two polymorphic forms of 1:2 INH–PABA cocrystals arose: Form I at 25 °C and Form II at-5 °C. Both polymorphic forms crystallized with prismatic habits.

2.2. Single crystal structure determination (SCSD)

Data collection of the INH cocrystals were performed at room temperature on an Agilent Super Nova diffractometer with CCD detector system equipped with a Mo source ($\lambda = 0.71073$ Å). Data integration, Lorentz-polarization effects and absorption corrections were performed with CrysAlisPro [32] (version 171.38.43 b). Using the Olex2 program [33], the structure was solved by direct methods and the model obtained was refined by full–matrix least squares on F^2 (SHELXTL–97) [34]. All C–H hydrogen atoms were placed in calculated positions and refined with fixed individual displacement parameters [$U_{iso}(H) = 1.2U_{eq}$] according to the riding model (C–H bond lengths of 0.93 Å) [34]. Mixed models were used for the treatment of hydrogen atoms attached to N and O atoms. Molecular representations were generated by Olex2 [33] and MERCURY 3.9 [35]. The CIF files of all structures were deposit in the Cambridge Structural Data Base [36] under the codes CCDC 1554637, 1554639, 1554640 and 1554641. Copies of the data can be obtained, free of charge, via www.ccdc.cam.ac.uk.

2.3. Powder X-ray diffraction (PXRD)

Data were recorded at room temperature on a Rigaku Ultima IV diffractometer, in Bragg-Brentano reflective geometry, with CuKα radiation ($\lambda = 1.5406$ Å) at 40 kV – 30 mA and Ni filter. The diffractograms were acquired in the 3–80° 2θ range with a step width of 0.02° and a constant counting time of 5 s per step.

2.4. Hirshfeld Surfaces (HS) and derived fingerprint plots

Hirshfeld surface analysis was used for the examination of the different types of interactions within the crystal structures of the INH cocrystals, showing the areas susceptible to weak and strong interactions. The 2-dimensional fingerprint plots, derived from the 3-dimensional d_{norm} Hirshfeld surfaces were generated using the software Crystal Explorer 3.1 [37] and both are illustrated in Fig. S2. Fig. S3 shows the comparative percentage in bars of the different types of contacts occurring in the INH cocrystals.

2.5. Vibrational spectroscopy

Fourier Transform infrared (FT-IR) spectra were recorded on a Bruker Vertex 70v spectrometer equipped with ATR accessory in the range of 4000 – 400 cm^{-1}, with an average of 256 scans and 2 cm^{-1} of spectral resolution.

2.6. Thermal analysis

Thermogravimetric Analyses (TGA) were carried out on a Shimadzu TGA-60 thermobalance. Approximately 5.0 mg of the samples were placed in open alumina pans and heated under N_2 flow from 25 to 600 °C at a heating rate of 10 °C/min. The Differential Scanning Calorimetry (DSC) was performed on Shimadzu DSC-60 instrument. The samples (2.5 ± 0.5 mg) were placed in open aluminum pans and heated from 25 to 400 °C under a N_2 atmosphere. The heating rate was set to 10 °C/min. According to TGA data, these experiments have been performed up to before the degradation temperature of each compound. The resulting data were analyzed using the Shimadzu TA-60 software (version 2.2).

2.7. Hot-Stage polarized optical microscopy

All Hot-Stage Microscopy (HSM) examinations were performed on a Linkam T95-PE device coupled to a Leica DM2500P optical microscope. Images were recorded using a CCD camera attached to the microscope at time intervals of 10 s. Single crystals of INH cocrystals were heated at a constant rate of 10 °C/min over a temperature range from 30 °C until the melting or the decomposition of the crystals. Both heating and acquisition of the images

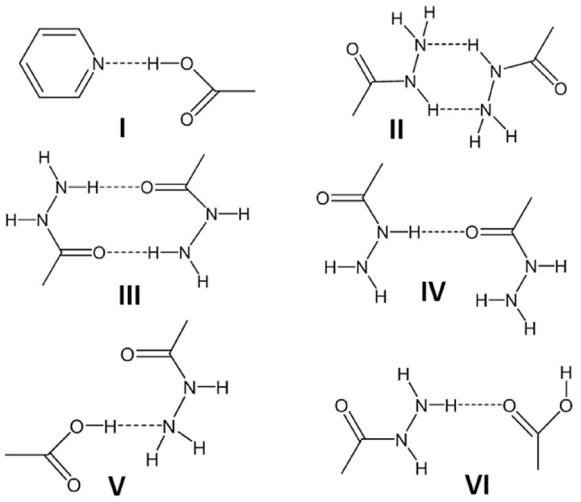

Fig. 1. Main Hydrogen Bonding Homo and Heterosynthons in INH cocrystal structures.

Table 1
Calculated ΔpKa between INH and carboxylic acid coformers.

Compound	pKa	ΔpKa = (pK_a (INH) − pK_a (acid))
Isoniazid	3.50	–
p-nitrobenzoic acid	3.43	0.07
p-cyanobenzoic acid	3.55	−0.05
p-aminobenzoic acid	2.38	1.12

were controlled by the Lynksys 32 software package (version 1.96).

3. Result and discussion

3.1. Structural description

INH is a weak base that contains two main functional groups in its structure: hydrazide and pyridine ring. Both groups are excellent hydrogen bond acceptors to form acid···pyridine (COOH···N_{arom}) and acid···hydrazide (COOH···$N_{hydrazide}$) heterosynthons. Moreover, the hydrazide group has also good hydrogen bond acceptor atoms (O and N) as well as donors which could generate hydrazide···hydrazide homosynthon. Fig. 1 shows the main hydrogen bonding supramolecular synthons (homo and heterosynthons) found to INH cocrystals with carboxylic acids. In a survey of the Cambridge Structural Database (CSD) [36], 39 INH cocrystals structures with coformers containing COOH groups have been identified showing that they represent about 40% of all INH structures deposited in CSD. Among the synthons represented in Fig. 1, the acid···pyridine (I) is the most recurrent being present in approximately 87% of the structures. In turn, the homosynthons II, III and IV are found in 18%, 36% and 18%, respectively. Finally, the heterosynthons V and VI appear in 8% and 31%, respectively, in the INH structures with carboxylic acids reported to date. In order to reproduce these acid···pyridine and acid···hydrazine heterosynthons, and based on the pK_a value of pyridine nitrogen of INH (pK_a = 3.50) [38], only aromatic acids containing COOH groups that agree with the "pK_a rule" for cocrystal, *i. d* $\Delta pK_a = pK_{a\,(base)} - pK_{a\,(acid)} < 0$ or between 0 and 3 [39,40], were selected for the cocrystallization experiments. The cocrystal formation was investigated using three acids with the following pK_a values: *p*-nitrobenzoic acid (pK_a = 3.43), *p*-cyanobenzoic acid (pK_a = 3.55) and *p*-aminobenzoic acid (pK_a = 2.38). As result, INH−PNBA, INH−PCNBA and two polymorphs of INH−PABA (Form I and II) were obtained. Table 1 presents the calculated ΔpKa values between INH and their respective carboxylic acid coformers.

Cocrystal formation was clearly identified by measuring the C−O bond length differences of the carboxyl groups in the acid molecules ($\Delta D_{C\text{-}O}$). It is stated that if this difference is smaller than 0.03 Å, the salt formation is expected. On the other hand, if this variation is high (>0.08 Å), then a cocrystal is formed [40,41]. The $\Delta D_{C\text{-}O}$ values founded for all INH structures depicted here are higher than 0.08 Å (INH-PNBA = 0.098 (1) Å; INH-PCNBA = 0.108 (2) Å; INH-PABA-I = 0.104 (5) and 0.115 (5); INH-PABA-II = 0.110 (2) and 0.102 (2)), which means that the C−O distances are not symmetrical, as in the carboxylate anions, evidencing a cocrystal formation. Fig. S1 shows the asymmetric unit (ASU) of INH cocrystals. A detailed description of each crystal structure is provided below. The crystallographic data and the geometric parameters of the H-bonds are summarized in Tables 2 and 3, respectively.

3.1.1. INH−PNBA

This cocrystal crystallized in the triclinic $P\bar{1}$ space group. The asymmetric unit (ASU) of this cocrystal (Fig. S1a) consists of one

Table 2
Crystallographic parameters of INH cocrystals.

Identification code	INH-PNBA	INH-PCNBA	INH-PABA-I	INH-PABA-II
Empirical formula	$C_{13}H_{12}N_4O_5$	$C_{14}H_{12}N_4O_3$	$C_{20}H_{21}N_5O_5$	$C_{20}H_{21}N_5O_5$
Formula weight	304.27	284.28	411.42	411.42
Temperature (K)	293 (2)	293 (2)	293 (2)	293 (2)
Crystal system	Triclinic	Triclinic	Monoclinic	Monoclinic
Space group	$P\bar{1}$	$P\bar{1}$	$P2_1$	$P2_1/c$
a (Å)	7.0573 (5)	7.0549 (5)	12.9772 (10)	16.2167 (5)
b (Å)	7.1868 (6)	7.1844 (6)	5.0685 (3)	5.08592 (11)
c (Å)	14.9643 (8)	15.2175 (12)	16.0931 (11)	25.4781 (6)
α (°)	91.375 (6)	81.660 (6)	90	90
β (°)	98.592 (5)	81.845 (6)	108.818 (8)	107.990 (3)
γ (°)	116.362 (7)	63.035 (8)	90	90
Volume (Å)^3	668.92 (9)	677.64 (10)	1001.94 (12)	1998.62 (9)
Z/Z′	2/1	2/1	2/1	4/1
ρ_{calc} (g cm^3)	1.511	1.393	1.364	1.367
μ (mm^{-1})	0.119	0.102	0.101	0.101
Reflections collected	11408	14281	11619	28914
Independent reflections	2922	2982	4042	4726
Unique reflections	2189	2444	3774	3780
R_1 [I ≥ 2σ(I)]	0.0509	0.0452	0.0485	0.0528
wR_2 [all data]	0.1453	0.1308	0.1247	1536
Goodness-of-fit on F^2	1.047	1.081	1.059	1.093

Table 3
Geometric parameters of the H-bonds in the INH cocrystals.

Interaction	D···A(Å)	H···A(Å)	D–H···A(°)	Symmetry Code
INH-PNBA				
O2–H2···N2	2.658 (2)	1.838 (1)	177.13 (11)	x,y,z
N3–H3A···O1	3.021 (3)	2.476 (2)	121.97 (10)	x,y,z
N1–H1···N3	2.911 (3)	2.168 (2)	144.46 (15)	−x + 2,−y + 1,−z + 2
N3–H3B···O5	3.208 (3)	2.467 (2)	144.66 (16)	x + 2,+y + 1,+z + 1
C3–H3···O3	3.222 (2)	2.577 (1)	126.83 (13)	x,y,z
INH-PCNBA				
O2–H2A···N2	2.658 (2)	1.818 (1)	174.42 (12)	x,y,z
N1–H1···N3	2.981 (2)	2.259 (1)	141.47 (15)	−x,−y + 2,−z + 2
N3–H3B···N4	3.270 (3)	2.515 (2)	135.85 (13)	−x + 1,−y + 2,−z + 1
N3–H3A···O1	3.150 (2)	2.295 (1)	170.81 (11)	x,y,z
C10–H10···N3	3.610 (3)	2.718 (2)	168.08 (13)	X + 1,+y,+z − 1
C3–H3···O3	3.319 (3)	2.690 (2)	125.64 (15)	x,y,z
C4–H4···O1	3.353 (3)	2.599 (2)	138.49 (13)	x + 1,+y,+z
C12–H12···O3	3.236 (2)	2.493 (2)	137.01 (15)	x + 1, +y, +z
INH-PABA-I				
O1–H2A···N2	2.731 (4)	1.916 (3)	171.76 (19)	x,y,z
O4–H4C···N3	2.819 (4)	2.190 (5)	148.96 (16)	x,y,z
N1–H1···O1	2.851 (3)	2.128 (2)	141.49 (19)	x,+y − 1,+z
N5–H5A···O3	2.992 (5)	2.180 (3)	155.81 (21)	−x + 1,+y − 1/2,−z + 2
N3–H3B···O1	3.218 (5)	2.454 (4)	143.34 (17)	−x + 1,+y − 1/2,−z + 2
N3–H3A···O5	3.091 (4)	2.239 (3)	169.46 (23)	x,+y + 1,+z
N4–H4A···N4	3.201 (5)	2.396 (4)	154.27 (26)	−x,+y − 1/2,−z
N4–H4B···O5	2.998 (5)	2.170 (4)	162.12 (20)	−x + 1,+y + 1/2,−z + 1
C4–H4···O2	3.365 (6)	2.581 (3)	142.27 (28)	−x + 1,+y − 1/2,−z + 1
C3–H3···O3	3.499 (4)	2.624 (3)	156.96 (24)	x,+y + 1,+z
C12–H12···O5	3.358 (4)	2.608 (3)	138.10 (21)	−x + 1,+y + 1/2,−z+1
C17–H17···O3	3.298 (5)	2.560 (3)	136.52 (20)	−x+1,+y − 1/2, −z+2
INH-PABA-II				
O2–H2A···N2	2.729 (3)	1.916 (2)	171.55 (13)	x,y,z
O4–H4A···N3	2.725 (3)	2.004 (2)	146.48 (13)	x,y,z
N1–H1···O1	2.878 (2)	2.164 (1)	140.12 (10)	x,+y − 1,+z
N3–H3A···O5	3.030 (2)	2.170 (2)	173.37 (12)	x,+y − 1,+z
N5–H5A···N4	3.179 (3)	2.366 (2)	157.76 (13)	x + 1,−y+1/2 + 1,+z − 1/2
N4–H4B···N5	3.168 (3)	2.348 (2)	159.56 (13)	x − 1,−y + 1/2,+z + 1/2
N5–H5B···O3	2.954 (2)	2.116 (2)	159.51 (14)	−x + 2,−y + 1,−z + 1
N3–H3B···O1	3.177 (2)	2.356 (2)	153.46 (13)	−x + 2,−y + 1,−z + 1
N4–H4C···O5	2.968 (2)	2.105 (2)	166.68 (12)	−x + 1,−y + 1,−z + 1
C12–H12···O5	3.461 (2)	2.738 (2)	135.25 (12)	−x + 1,−y + 1,−z + 1
C19–H19···O3	3.274 (2)	2.562 (2)	133.60 (12)	−x + 2,−y + 1,−z + 1
C4–H4···O3	3.519 (3)	2.633 (2)	159.39 (14)	x,+y + 1,+z

INH molecule and one *p*-nitrobenzoic acid (PNBA) molecule. The cocrystal was formed through O2–H2···N2 (2.658 (2) Å, 177.13 (11)°) and C3–H3···O3 (3.222 (2) Å, 126.83 (13)°) H-bonds involving the hydroxyl groups of PNBA and the pyridine one of INH to form an acid···pyridine heterosynthon (COOH···N_{arom}). In the cocrystal, INH molecules are arranged into chains along [100] direction by N1–H1···N3 (2.911 (3) Å, 144.46 (15)°) and N3–H3A···O1 (3.021 (3) Å, 121.97 (10)°) interactions that results in the $R_2^2(6)$ and $R_2^2(10)$ motifs, respectively (Fig. 2c). As result, INH and PNBA molecules are alternately present in the *ac* plane. Along the [010] direction, the PNBA molecules are associated to a INH chain by N3–H3B···O5 (3.208 (3) Å, 144.66 (16)°) H-bonds forming a layered structure (Fig. 2b). As expected, the crystal packing is stabilized by stacking of layers along the [010] direction through π-π stacking interactions between the INH and PNBA rings with intercentroid distance of 3.740 (3) Å (Fig. 2b).

3.1.2. INH–PCNBA

This cocrystal crystallizes in the triclinic $P\bar{1}$ space group with one INH molecule and one *p*-cyanobenzoic acid (PCNBA) molecule in the ASU (Fig. S1b). Similarly to INH–PNBA, the API and the coformer are associated by the acid···pyridine (COOH···N_{arom}) heterosynthon through O2–H2···N2 (2.658 (2) Å, 174.42 (12)°) and C3–H3···O3 (3.319 (3) Å, 125.64 (15)°) interactions. The INH and PCNBA molecules are also connected by N3–H3B···N4 (3.270 (3) Å, 135.85 (13)°) H-bonds involving the hydrazide and cyano groups. Thus, INH and PCNBA molecules are arranged into chains along the diagonal of *ac* direction (Fig. 3c). Moreover, along the [100] direction, these chains are oriented parallel to each other and are linked through C12–H12···O3 (3.236 (2) Å, 137.01 (15)) and C10–H10···N3 (3.610 (3) Å, 168.08 (13)°) interactions. Likewise, along the [010] direction, adjacent chains are related to each other by the hydrazide···hydrazide homosynthons ($R_2^2(6)$ and $R_2^2(10)$ graph set) from the association of INH molecules (Fig. 3c). As expected from the layered arrangement (Fig. 3b), the INH–PCNBA structure is stabilized by π···π interactions (3.777 (2) Å) formed between the aromatic centre of INH and acid molecules (Fig. 3c).

3.1.3. INH–PABA polymorphs

The crystals obtained from the reaction between INH and the coformer PABA in ethanol/acetonitrile (2:1 mixture) gave rise to the formation of two polymorphic cocrystals, namely INH–PABA-I and INH–PABA-II. The appearance of these polymorphic phases occurs simultaneously at different crystallization conditions. Thus, INH–PABA-I and INH–PABA-II can be considered concomitant polymorphs. The occurrence of both forms in the same crystallization medium can be explained by an interplay of kinetic and thermodynamic factors. The Form I was preferentially obtained at 25 °C while crystallization of Form II occurred at −5 °C. Thus, it was possible to separate these phases and analyze their structures.

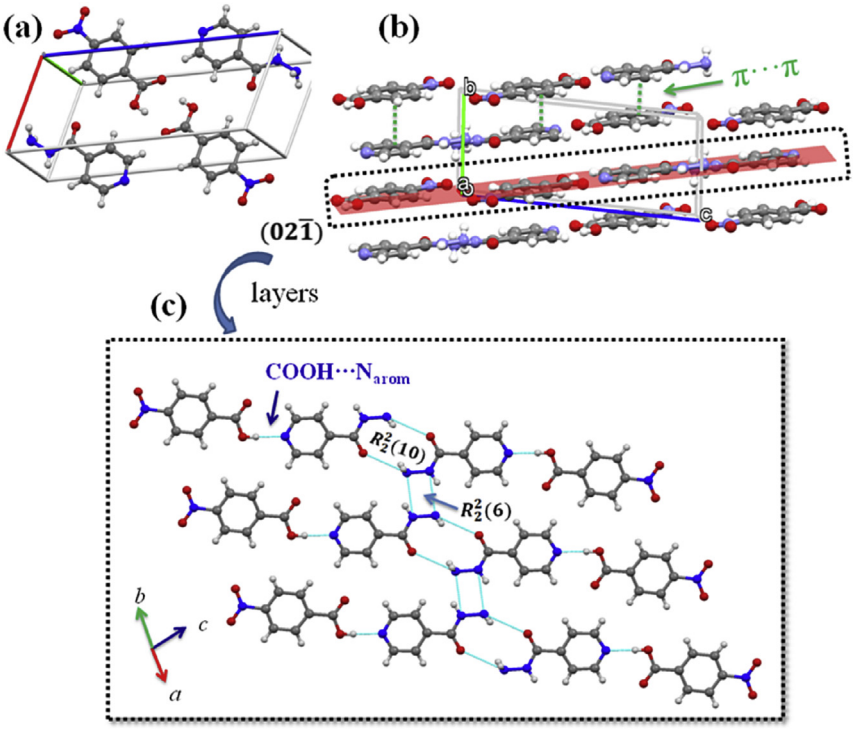

Fig. 2. (a) Packing view of the INH-PNBA Asymmetric Unit. (b) The layered structure is stabilized through π-π stacking interactions (in green). The molecular slice direction is indicated by a plane (in red). (c) Representation of the acid···pyridine heterosynthon (in blue) and hydrazide···hydrazide homosynthons ($R_2^2(6)$ and $R_2^2(10)$ motifs) which are extended along [100] direction. (For interpretation of the references to colour in this figure legend, the reader is referred to the web version of this article.)

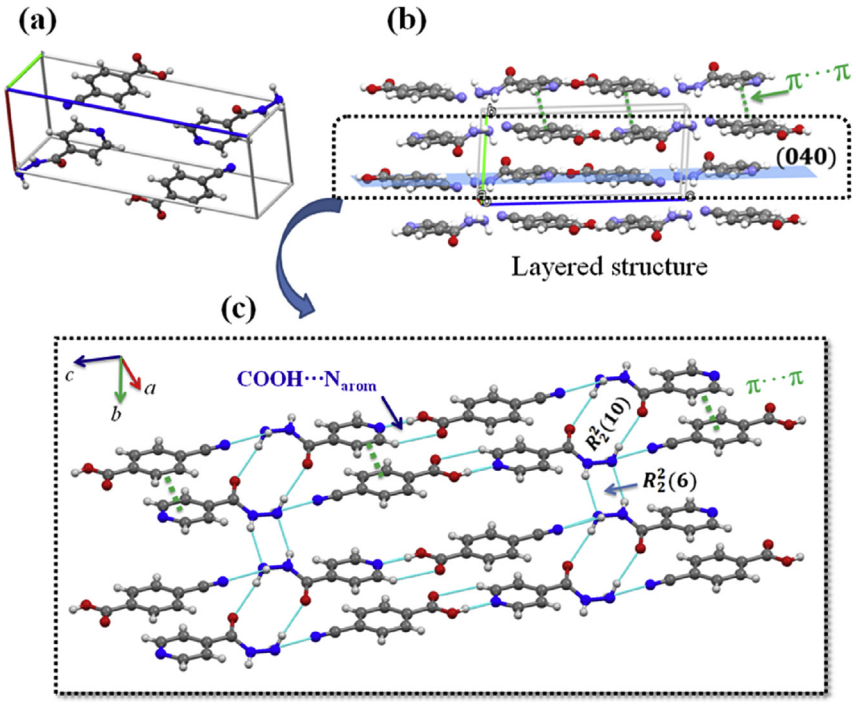

Fig. 3. (a) Packing view of the INH-PCNBA Asymmetric Unit. (b) Layered arrangement of the cocrystal. The molecular slice direction is indicated by a plane (in blue). (c) Representation of the acid···pyridine (in blue), hydrazide···hydrazide ($R_2^2(6)$ and $R_2^2(10)$ motifs) synthons and π-π stacking interactions (in green). (For interpretation of the references to colour in this figure legend, the reader is referred to the web version of this article.)

The INH−PABA-I crystallizes in the monoclinic space group $P2_1$, whereas the INH−PABA-II crystallizes in the monoclinic $P2_1/c$ space group. The ASU of both polymorphs consists of one INH molecule and two PABA molecules (namely as PABA-A and PABA-B). In both polymorphic forms, the PABA-A and INH molecules are associated by the acid···pyridine (COOH···N$_{arom}$) heterosynthon while PABA-B

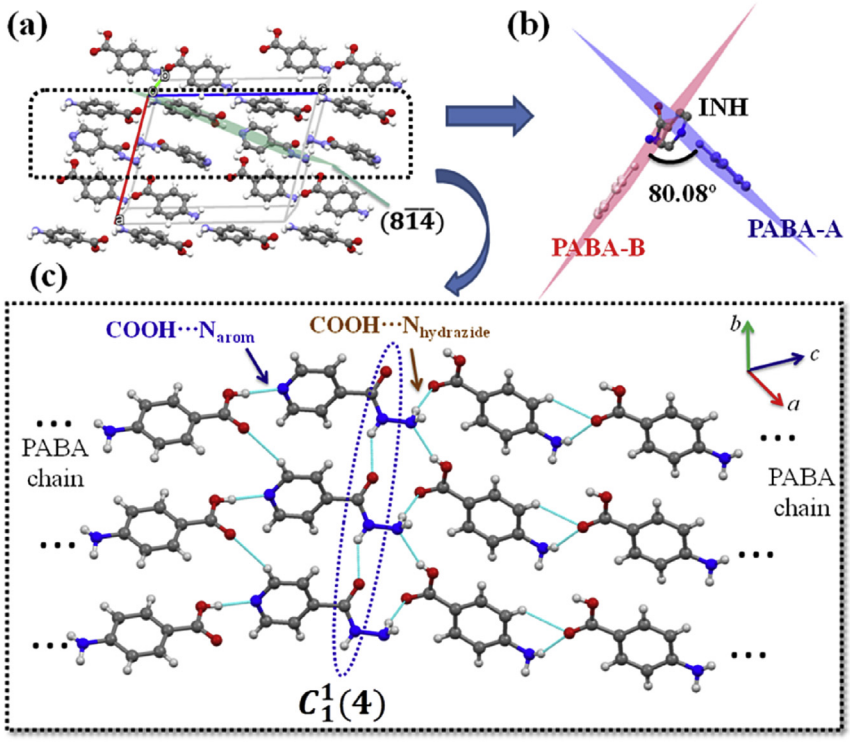

Fig. 4. (a) View of INH-PABA Form I packing along the *a* and *c* axis. The molecular slice direction is indicated by a plane (in dark green). (b) Orientation of molecules in the ASU showing that the mean plane of PABA-A and PABA-B molecules are 80.08°. (c) Representation of the acid···pyridine (in blue) and acid···hydrazide (in brown) heterosynthons. The INH and PABA chains are formed and extended through N–H···O H-bonds. (For interpretation of the references to colour in this figure legend, the reader is referred to the web version of this article.)

is H-bonded to INH by COOH···$N_{hydrazide}$ to form an acid···hidrazide heterosynthon (Figs. 4c and 5c). No conformational changes are observed between the INH molecules in the INH–PABA-I and INH–PABA-II structures (Fig. S5), allowing to conclude that this is a case of orientational polymorphism.

The polymorphs of INH–PABA have some structural similarities: (*i*) The *b* and *c* axis of INH–PABA-I, are similar to the *b* and *a* axis of INH–PABA-II, respectively (Table 2). (*ii*) Structurally, both

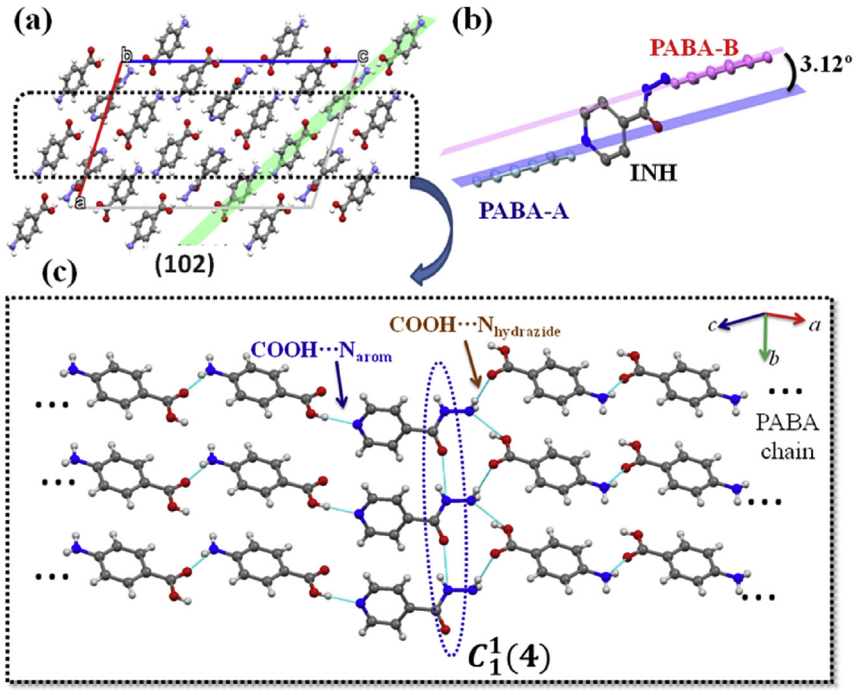

Fig. 5. (a) View of INH-PABA Form II packing along the *a* and *c* axis. The molecular slice direction is indicated by a plane (in light green). (b) Orientation of molecules in the ASU showing that the mean plane of PABA-A and PABA-B molecules are 3.12°. (c) Representation of the acid···pyridine (in blue) and acid···hydrazide (in brown) heterosynthons. The INH and PABA chains are formed and extended through N–H···O H-bonds. (For interpretation of the references to colour in this figure legend, the reader is referred to the web version of this article.)

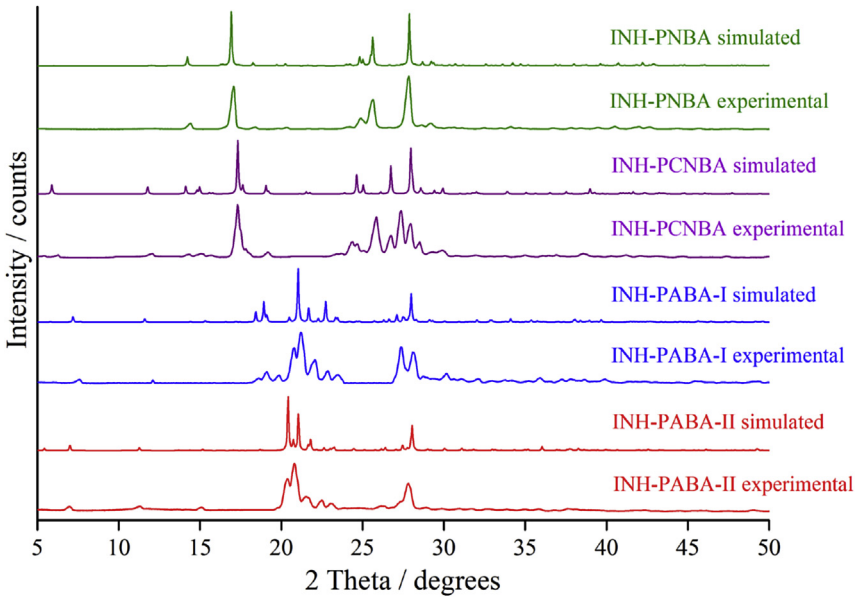

Fig. 6. Diffractograms of INH cocrystals. For all cocrystals, the experimental and calculated PXRD patterns show a good agreement, thus proving the purity and the homogeneity of the samples.

polymorphs show the presence of chains made only by PABA molecules as well as chains made only by INH molecules which are independents from each other. The INH molecules are connected between them by N1–H1···O1 interactions forming a $C_1^1(4)$ chain motif. Similarly, the PABA-A and PABA-B molecules are linked to each other through N–H···O H-bonds. These supramolecular motifs from INH–PABA-I and INH–PABA-II are shown in Figs. 4c and 5c, respectively. (*iii*) In the both structures the PABA chains are linked to INH molecules. However, the main difference between the polymorphs is related to the orientation of molecules in the ASU. In the INH–PABA-I the mean plane of PABA-A and PABA-B molecules are 80.08° (Fig. 4b), while in INH–PABA-II is around 3.12° (Fig. 5b). Moreover, along the PABA chains, the adjacent INH molecules are 73.37° oriented along [001] direction in INH–PABA-I, while in the INH–PABA-II the INH molecules are almost parallel each other (Fig. S6). The 3-D structure view along the *a* and *c* axis of INH–PABA polymorphs pointing out the features of each packing are shown in Figs. 4a and 5a.

3.2. Powder X-ray diffraction analysis

Powder X-ray diffraction is the most suitable characterization tool in establishing the completeness relative to the formation of novel crystalline forms [42]. Also, PXRD analysis confirms if the single crystal chosen for the data collection is representative of the whole sample. In this sense, this technique was used to verify the

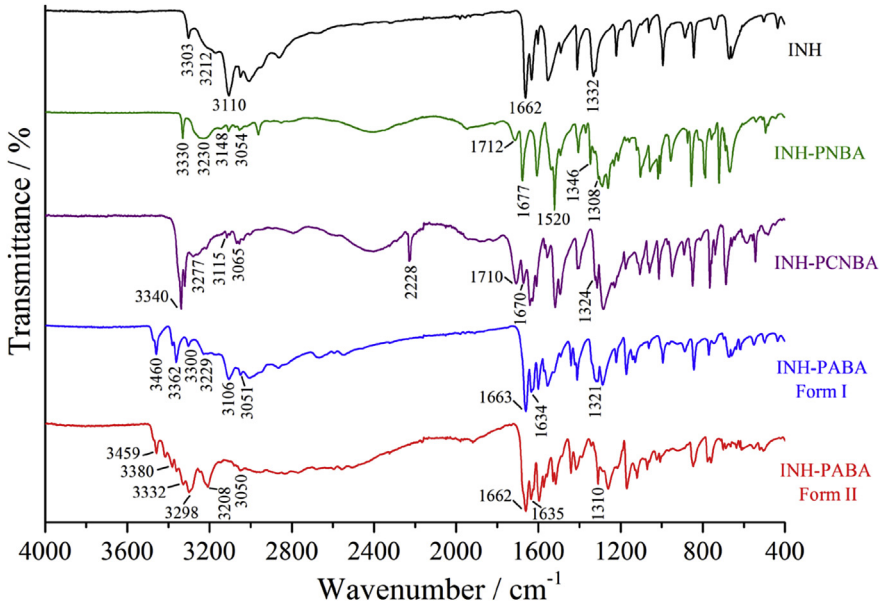

Fig. 7. FT-IR spectra of INH (black) and INH cocrystals: INH–PNBA (green), INH–PCNBA (purple), INH–PABA Form-I (blue) and INH–PABA Form-II (red). (For interpretation of the references to colour in this figure legend, the reader is referred to the web version of this article.)

Table 4
Principal FT-IR bands (cm^{-1}) for INH and INH cocrystals.

INH	INH-PNBA	INH-PCNBA	INH-PABA-I	INH-PABA-II	Assignment
_	3330	3340	3460	3459	$\nu(O-H)_{carboxyl}$
3303, 3212	3230, 3148	3277, 3115	3229,3106	3298, 3208	$\nu(N-H\ 1°)_{hydrazide}$
3110	3054	3065	3051	3050	$\nu(N-H\ 2°)_{hydrazide}$
_	–	–	3362, 3300	3380, 3232	$\nu(N-H\ 1°)_{amine}$
_	–	2228	–	–	$\nu(C\equiv N)_{cyano}$
_	1712	1710	1663	1662	$\nu(C=O)_{carboxyl}$
1662	1677	1670	1634	1335	$\nu(C=O)_{amide}$
_	1520	–	–	–	$\nu_a\ (N-O)_{nitro}$
_	1346	–	–	–	$\nu_s\ (N-O)_{nitro}$
1332	1308	1324	1321	1310	$\nu(C-N)_{pyridine}$

ν = stretching, a = antisymmetric, s = symmetric.

purity of the compounds. All INH cocrystals synthesized in the present study display experimental diffraction patterns in good agreement with the simulated ones, obtained from SCXRD analysis (Fig. 6), thus indicating that the obtained single crystals present high purity and representativity.

Additionally, the PXRD patterns analysis of INH–PABA polymorphs allowed to clearly and unambiguously differentiate them. Each experimental diffractogram revealed the presence of characteristic Bragg peaks, which are related to the formation of only one crystalline phase. Therefore, it is possible to state that the crystallization of INH–PABA forms I and II at different temperatures (25 °C and −5 °C) was an efficient procedure. In this sense, no Bragg peaks related to polymorph I were verified in the PXRD pattern of polymorph II (and vice versa).

3.3. Spectroscopy analysis

The FT-IR spectra of INH and its cocrystals (Fig. 7) were analyzed taking into account the structural features observed in the crystallographic study. Band assignments (Table 4) were performed using spectroscopic data available for cocrystals with carboxylic acids and related INH compounds found in the literature [24,26,27,29]. The cocrystal formations were identified by the evaluation of the changes in the vibrational modes of specific functional groups of the INH and the carboxylic acid coformers [43]. The functional groups in the INH molecule, among them hydrazide, amide and pyridine ring, exhibit IR stretching frequencies at 3303 cm^{-1} and 3212 cm^{-1} (primary amine NH stretches), 3110 cm^{-1} (secondary amine NH stretch), 1662 cm^{-1} (amide C=O stretch) and 1332 cm^{-1} (pyridine ring CN stretch). These stretching

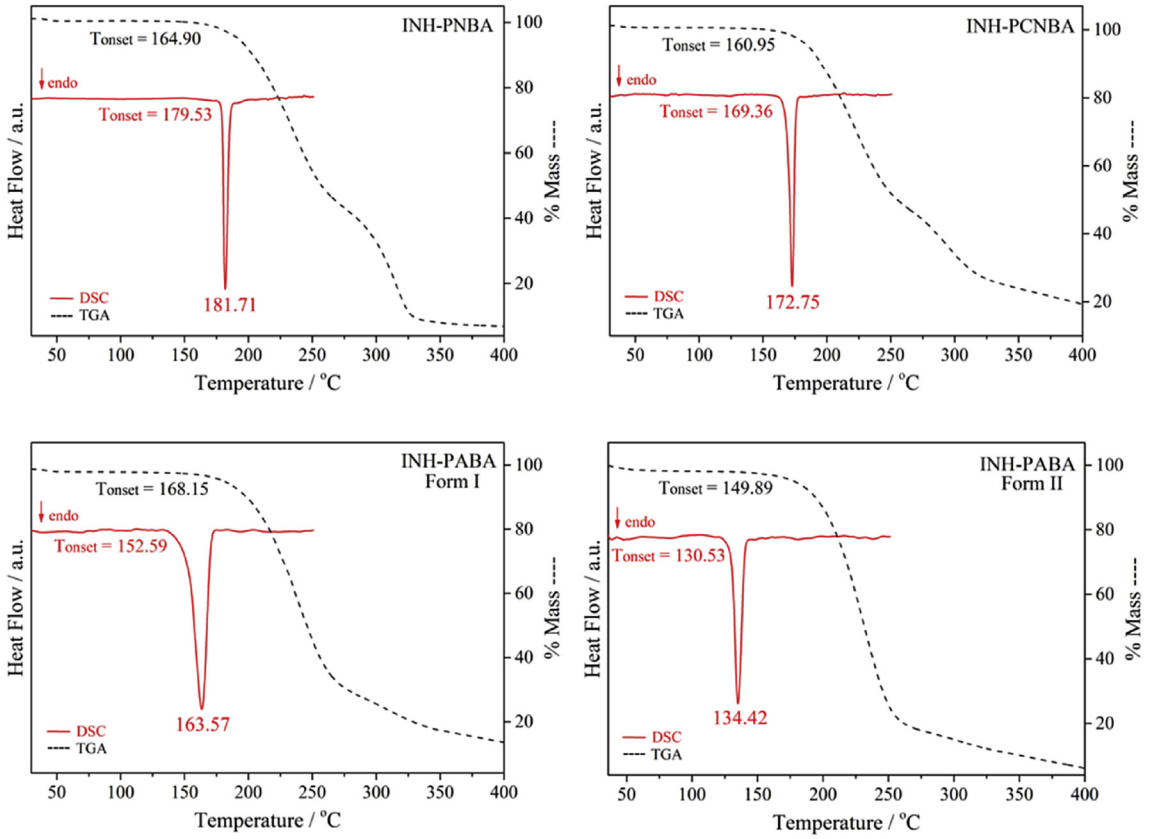

Fig. 8. DSC and TGA curves of INH cocrystals: INH–PNBA, INH–PCNBA, INH–PABA Form-I and INH–PABA Form-II.

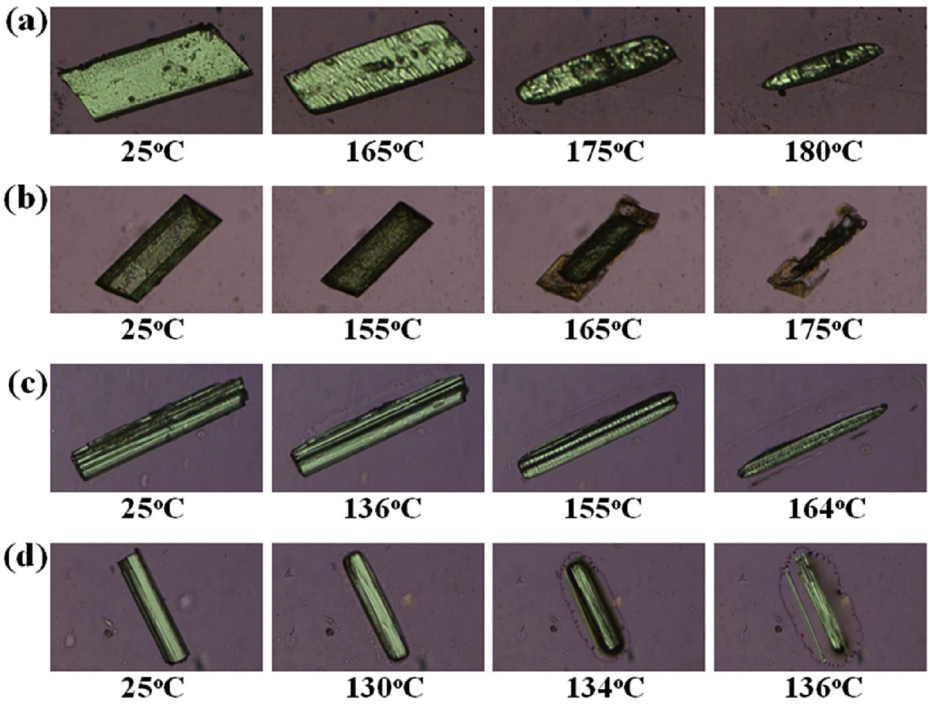

Fig. 9. Hot-stage microscopy images of INH–PNBA (a), INH–PCNBA (b), INH–PABA-Form-I (c) and INH–PABA-Form-II (d) single crystals.

frequencies appear shifted in the FT-IR spectra of all INH cocrystals, confirming the formation of novel solid forms.

According to the literature, primary amine shows two NH stretches (3400 – 3100 cm^{-1}), while secondary amine, shows only one NH stretch (3200 – 3000 cm^{-1}) [44]. In the INH FT-IR spectrum, the NH stretching vibrations attributed to primary amine appear as two bands at 3303 cm^{-1} and 3212 cm^{-1}. As expect, the NH stretching related to secondary amine is also observed as a single band at 3110 cm^{-1}. However, due to the formation of hydrogen bonding synthons involving the hydrazide group, the bands assigned to the NH stretching modes are observed shifted to lower wavenumbers in the cocrystals spectra.

The carboxylic acids, used as coformers, normally display two characteristic absorption bands at 3500–3300 cm^{-1} and 1750–1660 cm^{-1} related to the hydroxyl and carbonyl stretches of COOH group, respectively. These bands are observed in all cocrystals spectra: 3330 cm^{-1} and 1712 cm^{-1} (INH–PNBA), 3340 cm^{-1} and 1710 cm^{-1} (INH–PCNBA), 3460 cm^{-1} and 1663 cm^{-1} (INH–PABA Form-I) and 3459 cm^{-1} and 1662 cm^{-1} (INH–PABA Form-II). Concerning the pyridine ring, a strong band at 1662 cm^{-1}, assigned to the C–N stretching mode, is observed in the INH spectrum. In the cocrystals spectra, these bands appear shifted (8–28 cm^{-1}) due to the formation of acid···pyridine H-bonds. It is worth mentioning that the vibrational modes arising from the others functional groups such as nitro, cyano and amine, present in the acids molecules, could also be observed in the cocrystals spectra.

3.4. Thermal characterization

The thermal behavior of the INH cocrystals was studied by a combination of DSC, TGA and HSM techniques. The DSC/TGA curves of INH cocrystals are presented in Fig. 8. For comparison purpose, the DSC curve of INH was included (see Fig. S3). INH is stable between 25 and 160 °C and its DSC curve exhibits a single endothermic melting peak at 171 °C. DSC curves of INH–PNBA and INH–PCNBA are characterized by a single endothermic peak at 181.71 °C (T_{onset} = 179.53 °C) and 172.75 °C (T_{onset} = 169.36 °C), respectively, which were attributed to the fusion/decomposition of the samples. These values agree with the gradual mass loss that occurs in the TGA curves which begins at around 165 °C (sublimation of samples, T_{onset} = 164.90 °C) for INH–PNBA and 160 °C (T_{onset} = 160.95 °C) for INH–PCNBA.

The melting point of INH–PABA Form-I is assigned to an endothermic peak at 163.57 °C (T_{onset} = 152.59 °C) in the DSC curve. This event is accompanied by the thermal decomposition of the sample since a gradual mass loss in the TGA curve up to 170 °C (T_{onset} = 168.15 °C) can be observed. In comparison with the other cocrystals reported here, we found that INH–PABA Form II is the one with the lowest thermal stability. DSC curve of this polymorph showed an endothermic peak at 134.42 °C (T_{onset} = 130.53 °C), which was assigned to the melting process.

HSM was also performed in order to visualize the thermal events described above. Although HSM and DSC/TGA experiments were performed under different atmospheres, the results are in good agreement to each other. From HSM images (Fig. 9), it is possible to see that INH–PNBA and INH–PCNBA crystals undergo fusion/degradation at around 175 °C and 165 °C, respectively. The images also show the beginning of melting of the INH-PABA crystals which occur at around 164 °C for Form I and 136 °C for Form II. It is worth to mention that, according to DSC curves, there is no evidence of any other peaks that could be associated with any phase transition.

The thermal stability can be understood in terms of rupture of the crystal structure upon exposure to the heating process in an inert environment (experimental conditions in DSC/TGA experiments). Considering the thermal behavior of the INH–PABA polymorphs, it was observed that: (*i*) the higher melting point of INH–PABA Form I (Fig. 8) indicates that this polymorph is more stable than INH–PABA Form II, at room temperature (about 20 °C). (*ii*) No phase transition is observed in both polymorphs in the range between 25 °C and their respective melting points. (*iii*) The lower

heat of fusion of the lower melting INH-PABA-II (77.66 J g^{-1} in INH–PABA-II *vs.* 145.31 J g^{-1} in INH–PABA-I) indicates that the crystal forms are monotropically related (Heat of Fusion Rule) [45,46]. From this perspective, the following thermal stability order was established for INH cocrystals: INH–PABA-I > INH-PNBA > INH–PCNBA > INH–PABA-II. The degradation of the cocrystals INH–PNBA and INH–PCNBA are events that provide the rupture of structure and occur at lower temperatures when compared to INH–PABA-I. This aspect can be related to the reactivity of the PNBA and PCNBA coformers.

4. Conclusions

In this study, four cocrystals of the anti-tuberculosis drug Isoniazid (INH) were prepared and investigated using single crystal and powder X-ray diffraction, Hirshfeld surface analysis, FT-IR spectroscopy, thermogravimetry analysis, differential scanning calorimetry and Hot-Stage microscopy. These cocrystals were designed to explore the supramolecular synthons diversity between this API and aromatic carboxylic acids. Analysis of the crystal structures and packing revealed that the INH–PNBA and INH–PCNBA cocrystals are formed by acid···pyridine heterosynthons. In addition, their structures are also stabilized by hydrazide···hydrazide homosynthons and π-π stacking interactions. On the other hand, the INH–PABA polymorphs are formed through acid···pyridine and acid···hydrazide heterosynthons. This is a typical case of orientational polymorphism.

From the FT-IR spectra it was possible to confirm the cocrystal formation. The TGA/DSC results showed that the INH–PNBA and INH–PCNBA cocrystals undergo thermal degradation/fusion while INH-PABA polymorphs just melt and, according to the Heat of Fusion Rule, they are monotropically related. In relation to thermal stability, the following order was established for INH cocrystals: INH–PABA-I > INH–PNBA > INH–PCNBA > INH–PABA-II. As expected, these results are in good agreement with the HSM images. The present study shows that a better comprehension of the supramolecular features/interactions can be crucial for the development of more stable and efficient INH solid forms.

Acknowledgements

The authors acknowledge the Brazilian funding agencies FAPESP (L.F.D. grant 15/25694-0 and P.S.C.-Jr. grant 12/05616-7), CAPES (M.S.S., C.C.P.S.) and CNPq for financial support. The authors would also like to thank Dra. Charlane C. Correa (Universidade Federal de Juiz de Fora) and Dr. Alejandro Pedro Ayala (Universidade Federal do Ceará) for allowing access to the X-ray diffraction and FT-IR facilities, respectively.

Appendix A. Supplementary data

Supplementary data related to this article can be found at https://doi.org/10.1016/j.molstruc.2017.09.115.

References

[1] J. Wouters, L. Quere, D.E. Thurston, Pharmaceutical Salts and Co-crystals, Royal Society of Chemistry, 2011.
[2] D.P. Elder, R. Holm, H.L.d Diego, Use of pharmaceutical salts and cocrystals to address the issue of poor solubility, Int. J. Pharm. 453 (2013) 88–100.
[3] N. Shan, M.J. Zaworotko, The role of cocrystals in pharmaceutical science, Drug Discov. Today 13 (2008) 440–446.
[4] N.K. Duggirala, M.L. Perry, O. Almarsson, M.J. Zaworotko, Pharmaceutical cocrystals: along the path to improved medicines, Chem. Commun. 52 (2016) 640–655.
[5] G.R. Desiraju, Crystal engineering: from molecule to crystal, J. Am. Chem. Soc. 135 (2013) 9952–9967.
[6] L.F. Diniz, P.S. Carvalho, C.C. de Melo, J. Ellena, Development of a salt drug with improved solubility: ethionamide nitrate, J. Mol. Struct. 1137 (2017) 119–125.
[7] L.F. Diniz, P.S. Carvalho Jr., C.C. de Melo, J. Ellena, Reducing the hygroscopicity of the anti-tuberculosis drug (S, S)-ethambutol using multicomponent crystal forms, Cryst. Growth & Des. 17 (2017) 2622–2630.
[8] J.W. Steed, The role of co-crystals in pharmaceutical design, Trends Pharmacol. Sci. 34 (2013) 185–193.
[9] A.V. Trask, An overview of pharmaceutical cocrystals as intellectual property†, Mol. Pharm. 4 (2007) 301–309.
[10] N. Jouini, L. BenHamada, A. Jouini, Crystal structure of a new organic condensed phosphate (C 6 H 9 N 3 O) H 2 P 2 O 7, Mater. Res. Bull. 42 (2007) 56–63.
[11] A. Lemmerer, J. Bernstein, V. Kahlenberg, Hydrogen bonding patterns of the co-crystal containing the pharmaceutically active ingredient isoniazid and terephthalic acid, J. Chem. Crystallogr. 41 (2011) 991–997.
[12] S. Cherukuvada, A. Nangia, Fast dissolving eutectic compositions of two antitubercular drugs, CrystEngComm 14 (2012) 2579–2588.
[13] P. Grobelny, A. Mukherjee, G.R. Desiraju, Drug-drug co-crystals: temperature-dependent proton mobility in the molecular complex of isoniazid with 4-aminosalicylic acid, CrystEngComm 13 (2011) 4358–4364.
[14] A. Lemmerer, J. Bernstein, V. Kahlenberg, One-pot covalent and supramolecular synthesis of pharmaceutical co-crystals using the API isoniazid: a potential supramolecular reagent, CrystEngComm 12 (2010) 2856–2864.
[15] B. Lei, C.-J. Wei, S.-C. Tu, Action mechanism of antitubercular isoniazid Activation by Mycobacterium tuberculosis KatG, isolation, and characterization of InhA inhibitor, J. Biol. Chem. 275 (2000) 2520–2526.
[16] S. Singh, B. Mohan, A pilot stability study on four-drug fixed-dose combination anti-tuberculosis products, Int. J. Tuberc. Lung Dis. 7 (2003) 298–303.
[17] M.L. Bastos, H. Hussain, K. Weyer, L. Garcia-Garcia, V. Leimane, C.C. Leung, M. Narita, J.M. Penã, A. Ponce-de-Leon, K.J. Seung, Treatment outcomes of patients with multidrug-resistant and extensively drug-resistant tuberculosis according to drug susceptibility testing to first-and second-line drugs: an individual patient data meta-analysis, Clin. Infect. Dis. 59 (2014) 1364–1374.
[18] W. Hong-min, Z. Xiao-Hong, Association of drug susceptibility testing results for first-and second-line drugs with treatment outcomes in patients with multidrug-resistant and extensively drug-resistant tuberculosis, Clin. Infect. Dis. 60 (2015) 1285–1286.
[19] A. Haywood, M. Mangan, G. Grant, B. Glass, Extemporaneous isoniazid mixture: stability implications, J. Pharm. Pract. Res. 35 (2005) 181–182.
[20] H. Bhutani, T. Mariappan, S. Singh, An explanation for the physical instability of a marketed fixed dose combination (FDC) formulation containing isoniazid and ethambutol and proposed solutions, Drug Dev. ind. Pharm. 30 (2004) 667–672.
[21] C.S. Gautam, L. Saha, Fixed dose drug combinations (FDCs): rational or irrational: a view point, Br. J. Clin. Pharmacol. 65 (2008) 795–796.
[22] H. Bhutani, S. Singh, K.C. Jindal, A.K. Chakraborti, Mechanistic explanation to the catalysis by pyrazinamide and ethambutol of reaction between rifampicin and isoniazid in anti-TB FDCs, J. Pharm. Biomed. Anal. 39 (2005) 892–899.
[23] H. Bhutani, T. Mariappan, S. Singh, The physical and chemical stability of anti-tuberculosis fixed-dose combination products under accelerated climatic conditions, Int. J. Tuberc. Lung Dis. 8 (2004) 1073–1080.
[24] S. Aitipamula, A.B. Wong, P.S. Chow, R.B. Tan, Novel solid forms of the anti-tuberculosis drug, Isoniazid: ternary and polymorphic cocrystals, CrystEngComm 15 (2013) 5877–5887.
[25] I. Sarcevica, L. Orola, M.V. Veidis, A. Podjava, S. Belyakov, Crystal and molecular structure and stability of isoniazid cocrystals with selected carboxylic acids, Cryst. Growth & Des. 13 (2013) 1082–1090.
[26] B. Swapna, D. Maddileti, A. Nangia, Cocrystals of the tuberculosis drug isoniazid: polymorphism, isostructurality, and stability, Cryst. Growth & Des. 14 (2014) 5991–6005.
[27] S.M.A. Mashhadi, U. Yunus, M.H. Bhatti, M.N. Tahir, Isoniazid cocrystals with anti-oxidant hydroxy benzoic acids, J. Mol. Struct. 1076 (2014) 446–452.
[28] R. Kaur, S. Perumal, A.J. Bhattacharyya, S. Yashonath, T. Guru Row, Structural insights into proton conduction in gallic acid–isoniazid cocrystals, Cryst. Growth & Des. 14 (2014) 423–426.
[29] S.M.A. Mashhadi, U. Yunus, M.H. Bhatti, I. Ahmed, M.N. Tahir, Synthesis, characterization, solubility and stability studies of hydrate cocrystal of anti-tubercular Isoniazid with antioxidant and anti-bacterial Protocatechuic acid, J. Mol. Struct. 1117 (2016) 17–21.
[30] M. Oruganti, P. Khade, U.K. Das, D.R. Trivedi, The hierarchies of hydrogen bonds in salts/cocrystals of isoniazid and its Schiff base–a case study, RSC Adv. 6 (2016) 15868–15876.
[31] C.C. de Melo, P. de Sousa Carvalho, L.F. Diniz, R.F. D'Vries, A.P. Ayala, J. Ellena, Supramolecular synthesis and thermochemical investigations of pharmaceutical inorganic isoniazid salts, CrystEngComm 18 (2016) 6378–6388.
[32] A. Technologies (Ed.), Agilent, CrysAlis PRO, 2010. Yarnton, England.
[33] O.V. Dolomanov, L.J. Bourhis, R.J. Gildea, J.A.K. Howard, H. Puschmann, OLEX2: a complete structure solution, refinement and analysis program, J. Appl. Crystallogr. 42 (2009) 339–341.
[34] G. Sheldrick, A short history of SHELX, Acta Crystallogr. Sect. A 64 (2008) 112–122.
[35] C.F. Macrae, I.J. Bruno, J.A. Chisholm, P.R. Edgington, P. McCabe, E. Pidcock, L. Rodriguez-Monge, R. Taylor, J. van de Streek, P.A. Wood, Mercury CSD 2.0-new features for the visualization and investigation of crystal structures, J. Appl. Crystallogr. 41 (2008) 466–470.

[36] F. Allen, The Cambridge Structural Database: a quarter of a million crystal structures and rising, Acta Crystallogr. Sect. B 58 (2002) 380–388.
[37] J.J. McKinnon, M.A. Spackman, A.S. Mitchell, Novel tools for visualizing and exploring intermolecular interactions in molecular crystals, Acta Crystallogr. Sect. B 60 (2004) 627–668.
[38] W. Lund, The Pharmaceutical Codex: Principles and Practice of Pharmaceutics, The Pharmaceutical Press, London, 1994.
[39] B.R. Bhogala, S. Basavoju, A. Nangia, Tape and layer structures in cocrystals of some di- and tricarboxylic acids with 4,4[prime or minute]-bipyridines and isonicotinamide. From binary to ternary cocrystals, CrystEngComm 7 (2005) 551–562.
[40] S.L. Childs, G.P. Stahly, A. Park, The salt-cocrystal continuum: the influence of crystal structure on ionization state, Mol. Pharm. 4 (2007) 323–338.
[41] C.C. da Silva, R.d.O. Pepino, C.C. de Melo, J.C. Tenorio, J. Ellena, Controlled synthesis of new 5-fluorocytosine cocrystals based on the p K a rule, Cryst. Growth & Des. 14 (2014) 4383–4393.
[42] J.F. Remenar, M.L. Petersom, P.W. Stephens, Z. Zhang, Y. Zimenkov, M.B. Hickey, Celecoxib:nicotinamide dissociation: using excipients to capture the cocrystal's potential, Mol. Pharm. 4 (2007) 386–400.
[43] A. Heinz, C.J. Strachan, K.C. Gordon, T. Rades, Analysis of solid-state transformations of pharmaceutical compounds using vibrational spectroscopy, J. Pharm. Pharmacol. 61 (2009) 971–988.
[44] G.A. Giffin, S. Boesch, D.N. Bopege, D.R. Powell, R.A. Wheeler, R. Frech, Vibrational spectroscopy of secondary amine salts: 1. Assignment of NH2+ stretching frequencies in crystalline phases, J. Phys. Chem. B 113 (2009) 15914–15920.
[45] M.A. Burger, R. Ramberger, Acta [Wien] II, vol. 259, 1979.
[46] J. Bernstein, Polymorphism in Molecular Crystals, Clarendon Press, 2002.